Ferrimagnetic-antiferromagnetic phase transition in $Mn_{2-x}Cr_xSb$: Electronic structure and electrical and magnetic properties

J. H. Wijngaard* and C. Haas
Laboratory of Inorganic Chemistry, Materials Science Centre, University of Groningen, Nijenborgh 16, 9747 AG Groningen, The Netherlands

R. A. de Groot
Laboratory of Inorganic Chemistry, Materials Science Centre, University of Groningen, Nijenborgh 16, 9747 AG Groningen, The Netherlands
and Research Institute for Materials, Faculty of Science, Toernooiveld, 6525 ED Nijmegen, The Netherlands
(Received 11 September 1991)

Self-consistent spin-polarized energy-band calculations have been performed for Mn_2Sb for a ferrimagnetic (FI), ferromagnetic (F), and antiferromagnetic (AF) spin alignment. The calculated local moments on the two types of Mn atoms are in agreement with values obtained from neutron diffraction for FI Mn_2Sb. A comparison of the band structures of FI, F, and AF Mn_2Sb shows characteristic differences in hybridization between the Mn $3d$ orbitals and Sb $5p$ orbitals. The covalent interactions between Mn(1) and Mn(2) $3d$ orbitals are responsible for a strong direct antiferromagnetic exchange within the triple layers Mn(2)-Mn(1)-Mn(2). The exchange between triple layers is attributed to a much weaker indirect exchange via Sb $5p$ states. We also carried out measurements of the magnetic properties and the electrical transport properties (resistivity, Seebeck effect, Hall effect) of single crystals and polycrystalline samples of Mn_2Sb and $Mn_{2-x}Cr_xSb$ ($x<0.2$). The Cr-doped samples show a phase transition from an AF to a FI state. This phase transition is associated with strong changes of the electrical transport properties. We have analyzed these changes in terms of the calculated band structures of FI and AF Mn_2Sb.

I. INTRODUCTION

Mn_2Sb is a ferrimagnetic compound with a Curie temperature of 550 K. In the crystal structure there are two crystallographically different Mn atoms, Mn(1) and Mn(2), with magnetic moments which are antiparallel in the ferrimagnetic state.[1-4] The magnetic properties change drastically if part of the Mn atoms are substituted.[5-12] The compounds $Mn_{2-x}Cr_xSb$ with $0.01<x<0.25$ show a first-order phase transition from the ferrimagnetic state to an antiferromagnetic state. The phase-transition temperature T_s increases with increasing Cr content x, and can be changed by applying a magnetic field. Neutron-diffraction studies show the presence of triple layers Mn(2)-Mn(1)-Mn(2) with antiparallel magnetic moments on Mn(1) and Mn(2) in both the ferrimagnetic and antiferromagnetic states.[2-4,8,9] In the ferrimagnetic state the moments of all triple layers are parallel, whereas the ordering is antiparallel in the antiferromagnetic state. For very small Cr content ($x<0.035$), an intermediate phase with a spiral spin configuration is found.[8,10] The temperature dependence of the sublattice magnetizations and the magnetic anisotropy of Mn_2Sb and Sn-, Cr-, and Fe-substituted Mn_2Sb has been studied extensively using NMR and Mössbauer techniques.[13-19] The spin-wave dispersion of Mn_2Sb and $Mn_{2-x}Cr_xSb$ has been measured with inelastic neutron scattering.[20,21]

The electrical and thermal transport properties are also influenced by the phase transition. Changes up to 13% in the electrical conductivity and 11% in the thermal conductivity are reported by Sato *et al.*[22] when going through the phase transition by applying a magnetic field. This makes it possible to use the compound as a thermal switch.

The Cr substitution does not alter the crystal structure, but it changes the lattice parameters. Moreover, the phase transition is accompanied by discontinuities in the crystallographic a and c axes. The value of the c axis at which the discontinuity appears is about the same for all values of the Cr content x, and is equal to $c_0=6.53$ Å.[10] These observations suggest that the phase transition is driven by a strong dependence of the exchange interactions on the interatomic distances.

In a discussion of the phase transition in $Mn_{2-x}Cr_xSb$, Kittel[23] treated the magnetic structure as consisting of two equivalent magnetic sublattices A and B. Each sublattice represents a set of triple layers Mn(2)-Mn(1)-Mn(2). The exchange interactions within a triple layer are assumed to be strong. The central assumption of the model is that the exchange interaction between A and B is rather weak and is a linear function of the lattice parameter c, and that it becomes zero at a critical value c_0. Because of the temperature dependence of the lattice parameters, a phase transition from an antiferromagnetic structure to a ferrimagnetic structure will occur at the temperature T_s where $c=c_0$. The lattice parameters also depend on the Cr content x, as observed. Thus, the role

of Cr is not to induce directly a change of the strength or sign of the exchange interaction, but rather to induce changes of the lattice parameters. The model of Kittel makes it possible to explain the observed shift of the transition temperature T_s with an applied magnetic field. For a quantitative explanation of the observed magnetic properties, a more detailed theory is necessary.[24]

It is remarkable that, in spite of the interesting phase transition in Cr-substituted Mn_2Sb, only a few not very detailed studies of the magnetic and electrical properties have been reported in the literature. In this paper we report some experimental results of the electrical resistivity, the Seebeck effect, and the Hall effect as a function of temperature and applied magnetic field for $Mn_{2-x}Cr_xSb$. We also presented *ab initio* spin-polarized band-structure calculations on Mn_2Sb. The calculations were carried out for the ferrimagnetic, ferromagnetic, and antiferromagnetic states of Mn_2Sb, in order to gain insight in the nature of the magnetic interactions (direct versus indirect exchange). We discuss the electrical transport properties in terms of the calculated electronic structure.

II. EXPERIMENTAL PART

A. Synthesis and crystal structure

In order to synthesize $Mn_{2-x}Cr_xSb$, appropriate amounts of the pure elements were mixed in an alumina crucible, which was put inside a quartz tube. The quartz tube was evacuated, sealed, and gradually heated up to 900 °C in a Bridgman furnace. The temperature was kept at 900 °C for 1 day. Then the temperature was raised to 955 °C (just above the melting point of 948 °C of Mn_2Sb). The temperature of the alumina crucible was slowly lowered by transport of the tube in the temperature gradient of the furnace. After 2 days the temperature of the crucible had reduced to 900 °C. After this the temperature was lowered to room temperature in about 3 days. By this procedure it was possible to grow good single crystals of $Mn_{2-x}Cr_xSb$. The crystals showed easy cleavage parallel to the a-b plane.

Mn_2Sb has a tetragonal crystal structure of the Cu_2Sb type, with space group $P4/nmm$.[1,2] The lattice constants at room temperature are $a=4.08$ Å and $c=6.56$ Å. The Mn atoms occupy two different crystallographic positions Mn(1) (0,0,0), $(\frac{1}{2},\frac{1}{2},0)$ and Mn(2) $(0,\frac{1}{2},z)$, $(\frac{1}{2},0,-z)$ with $z=0.295$. The Sb atoms are at positions $(0,\frac{1}{2},z')$, $(\frac{1}{2},0,-z')$ with $z'=0.280$. The crystallographic unit cell, and also the ordering of the magnetic moments in the ferrimagnetic and antiferromagnetic phases, are shown in Fig. 1. The crystal structure of $Mn_{2-x}Cr_xSb$ is the same as that of Mn_2Sb, with a disordered distribution of the Cr atoms.

All synthesized samples were investigated by x-ray powder diffraction, and showed the Cu_2Sb-type structure. The observed dependence of the lattice parameters on the Cr content x agrees with data reported in the literature.[10] The spatial distribution of Cr in large samples is rather inhomogeneous, as a result of the method of preparation. Therefore, we used for the measurements rather small samples in which the Cr content is constant. The homogeneity of the Cr concentration is easily checked by resistivity measurements because only homogeneous samples show a sharp phase transition.

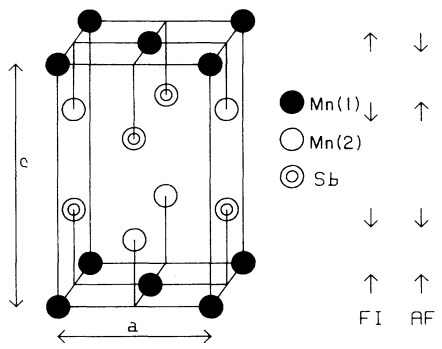

FIG. 1. Crystal structure of Mn_2Sb. The arrows indicate the ordering of the magnetic moments in the ferrimagnetic (FI) and antiferromagnetic (AF) phases.

B. Magnetic properties

Magnetization measurements of $Mn_{2-x}Cr_xSb$ samples were carried out as a function of the applied magnetic induction B_a (up to 5 T) at temperatures between 4 and 340 K, using a Faraday balance. The spontaneous magnetization $\mu_0 M_s$ was determined by extrapolating the high-field part of the magnetization isotherm to the value of the applied induction $B_a=\mu_0 H_a=N_d\mu_0 M$, where μ_0 is the vacuum permeability and N_d is the demagnetizing factor.

Results for the spontaneous magnetization of single crystals of Mn_2Sb and $Mn_{1.95}Cr_{0.05}Sb$ as a function of the temperature are shown in Fig. 2. The spontaneous magnetization of Mn_2Sb extrapolated to $T=0$ is 0.36 T. This value corresponds to an average magnetic moment of $0.85\mu_B$ per manganese atom, in good agreement with the value of $0.87\mu_B$ reported by Wilkinson *et al.*[2] The magnetization data for $Mn_{1.95}Cr_{0.05}Sb$ show a sharp transition at $T_s=177$ K. Below T_s there remains a small temperature-independent magnetization of 0.025 T, which is probably due to the presence of a small amount ($\sim 2\%$) of ferromagnetic MnSb which seems to be present as a second phase in all Cr-doped Mn_2Sb samples.[10,25]

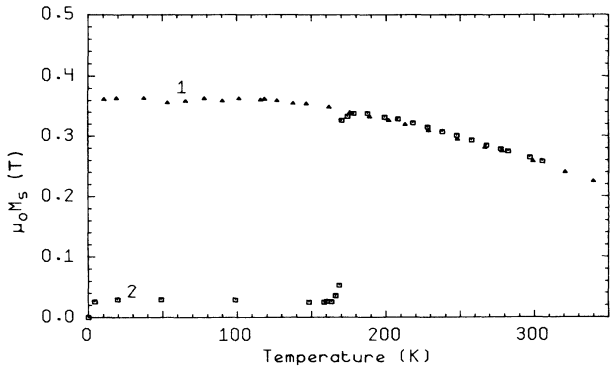

FIG. 2. Spontaneous magnetization of single crystals of Mn_2Sb (curve 1) and $Mn_{1.95}Cr_{0.05}Sb$ (curve 2).

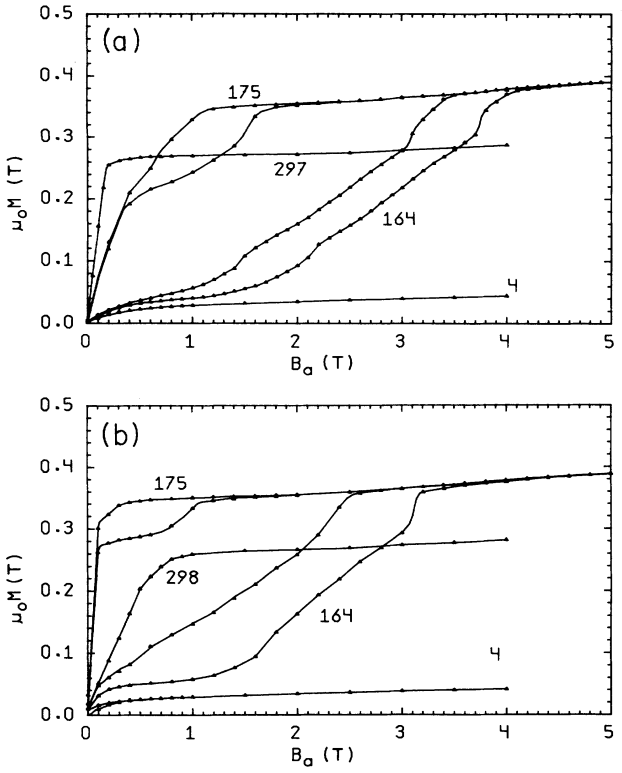

FIG. 3. Magnetization of $Mn_{1.95}Cr_{0.05}Sb$ as a function of an applied magnetic field (a) parallel or (b) perpendicular to the c axis. The numbers in the figure indicate the absolute temperature.

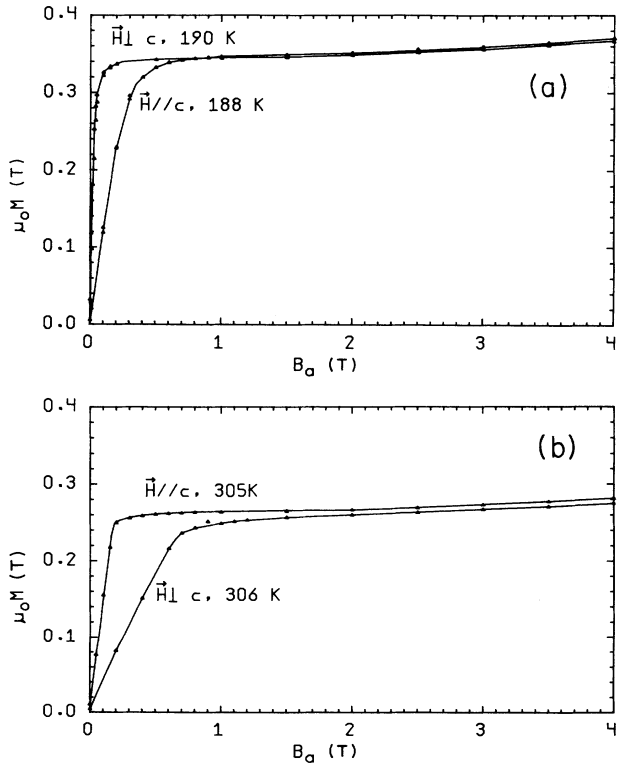

FIG. 4. Magnetization curves of $Mn_{1.95}Cr_{0.05}Sb$ showing a preferred orientation of the magnetization parallel to the c axis at 305 K, and perpendicular to the c axis at 188 K.

The magnetization of $Mn_{1.95}Cr_{0.05}Sb$ as a function of an applied field is shown in Fig. 3. At low temperatures we observe again a small magnetization due to MnSb. At temperatures slightly above the transition temperature $T_s = 177$ K, the change from the antiferromagnetic to the ferrimagnetic state can be induced by an applied magnetic field. However, it is evident that the change of the magnetization is a complicated phenomenon which cannot be explained quantitatively with the simple model of exchange inversion proposed by Kittel.[23]

A comparison of magnetization measurements with applied fields parallel and perpendicular to the c axis shows a change of the preferred orientation of the magnetization at a spin-flip temperature $T_0 = 240$ K in Mn_2Sb, and at $T_0 = 198$ K for $Mn_{1.95}Cr_{0.05}Sb$ (see Fig. 4), in agreement with results reported in the literature.[10]

C. Electrical resistivity and Seebeck effect

Electrical resistivity measurements on single crystals and polycrystalline samples were carried out using the four-point method. The contacts to the sample were made using a suspension of silver in methyl-isobutyl ketone. For the measurements of the Seebeck effect, the sample was clamped between gold contacts and a temperature gradient of 1 K was applied. A correction was made for the contribution of the gold contacts.

The electrical resistivity of $Mn_{2-x}Cr_xSb$ polycrystalline samples and single crystals was measured as a function of the temperature. The measurements on single crystals were carried out for a current in the plane perpendicular to the c axis. The data (Fig. 5) clearly show an abrupt change of the resistivity at the temperature T_s of the phase transition from the ferrimagnetic to the antiferromagnetic structure. We did not observe significant differences between the electrical resistivity of single crystals and polycrystalline samples.

The magnitude of the jump in the resistivity at T_s is nearly independent of x. This indicates that the increase in the resistivity in the antiferromagnetic state as compared to the ferrimagnetic state is due to the difference in magnetic order and is not due to the presence of chromium atoms as additional scattering centers. The residual resistivity (ρ at $T = 0$), on the other hand, increases

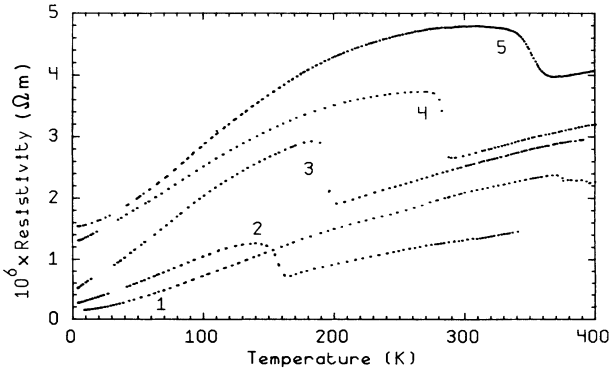

FIG. 5. Electrical resistivity of $Mn_{2-x}Cr_xSb$ samples. Curves 1, 3, and 5 are for polycrystalline samples with $x = 0$, 0.05, and 0.19, respectively, curves 2 and 4 for single crystals with $x = 0.03$ and 0.08, respectively.

strongly with increasing Cr content and is attributed to scattering of the charge carriers at Cr atoms.

Figure 6 shows magnetoresistivity data for a single crystal $Mn_{1.96}Cr_{0.04}Sb$ for an electrical current perpendicular to the c axis and a magnetic field parallel to the c axis. The large change of the resistivity near T_s is due to the field-induced transition from the antiferromagnetic to the ferrimagnetic state. At 157 K the transition is completed for an applied field of 2.7 T. There is a large hysteresis in the resistivity, as expected. Below 152 and above 165 K the change of the resistivity with magnetic field is small. The magnetoresistance data are consistent with the behavior expected from magnetic measurements.

In Fig. 7 typical results of measurements of the Seebeck effect of $Mn_{2-x}Cr_xSb$ are given. We find that the Seebeck effect of single crystals depends only slightly on the orientation of the temperature gradient with respect to the c axis. Moreover, the Seebeck effect of polycrystalline samples is nearly the same as that of single crystals.

The observed data show a small positive Seebeck coefficient of Mn_2Sb, indicating the presence of holes. Above the transition temperature T_s the Seebeck effect of $Mn_{2-x}Cr_xSb$ approaches that of Mn_2Sb. The Seebeck effect changes at T_s and becomes strongly negative below T_s. This change is attributed to the different magnetic structure; if it were due directly to the chromium atoms, one would expect a change proportional to the chromium content, which is not observed.

D. Hall effect

The Hall resistivity of magnetic materials is given by the relation

$$\rho_{xy}=E_y/j_x=R_0B_z^i+R_s\mu_0M_z\ , \tag{1}$$

where E_y is the Hall electrical field, j_x is the current, B_z^i is the internal magnetic induction, M_z is the magnetization, and μ_0 is the vacuum permeability.[26] The first term is the normal Hall effect, the coefficient R_0 is given approximately by $R_0=-1/ne$ (electron conduction) or $R_0=+1/pe$ (hole conduction). The second term in Eq. (1) represents the anomalous Hall effect caused by asymmetric scattering of the charge carriers (skew scattering and side jump contributions).

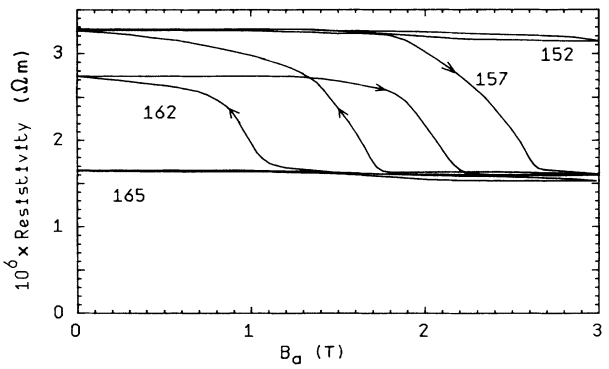

FIG. 6. Magnetoresistance of a single crystal $Mn_{1.96}Cr_{0.04}Sb$ at various temperatures. The electrical current was perpendicular to the c axis, the magnetic field was parallel to the c axis.

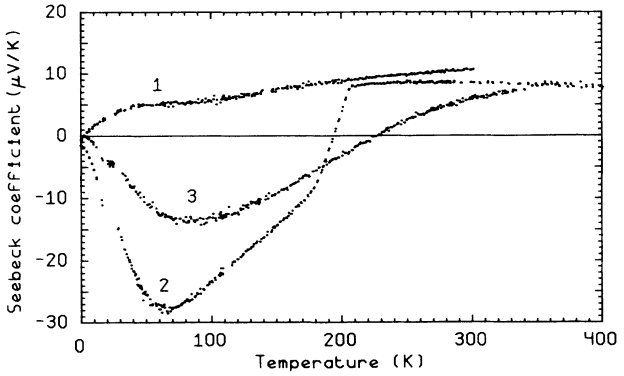

FIG. 7. Seebeck effect of polycrystalline $Mn_{2-x}Cr_xSb$ for (1) $x=0$, (2) $x=0.05$, and (3) $x=0.19$.

The Hall effect measurements were carried out in a helium-cooled cryostat, using a five-point method. Magnetic fields up to 3 T were available using a superconducting magnet. A 83-Hz ac current was applied to the sample, and the Hall effect was measured with a PAR lock-in amplifier.[27] The normal and anomalous Hall coefficients R_0 and R_s were calculated from the Hall resistivity and magnetic measurements using the method described by Otto.[27,28]

Typical Hall resistivity data for an applied magnetic field parallel to the c axis is shown in Figs. 8 and 9 for single crystals Mn_2Sb and $Mn_{1.96}Cr_{0.04}Sb$. The observed Hall resistivity ρ_{xy} at 4 K is small and negative and is a linear function of the applied magnetic field. The nonlinear dependence of ρ_{xy} on B_z at higher temperatures is caused by the positive contribution of the anomalous Hall effect. In the curves for Mn_2Sb at 222 and 249 K, the change of the easy axis of magnetization from perpendicular to parallel to the c axis is easily observed. The Hall resistivity of Mn_2Sb begins to decrease above about 200 K, and it becomes negative above about 300 K.

The values of the Hall coefficients R_0 and R_s as a function of temperature calculated from these data are shown in Fig. 10. The results for R_0 are not very accurate because of the dominating contribution of the anomalous Hall effect. The normal Hall coefficient R_0 changes from negative values at low temperatures (electron conduction) to positive values at high temperatures (hole conduction).

It is interesting to note that, although the anomalous Hall effect is very different in the antiferromagnetic and the ferrimagnetic states, the coefficient R_s is approximately the same in the two phases. Thus, the change of R_sM_z is caused by the change of M_z at the transition.

The value of R_s at $T=0$ is small. For perfect crystals we expect $R_s=0$ at $T=0$ since R_s is caused by scattering of the charge carriers. We conclude that the contribution to R_s of skew scattering at the chromium atoms is small.

We have also measured the Hall resistivity of polycrystalline samples of Mn_2Sb and $Mn_{1.95}Cr_{0.05}Sb$ as a function of temperature and magnetic field. The results are quite complicated and difficult to interpret; details are given by Wijngaard.[29]

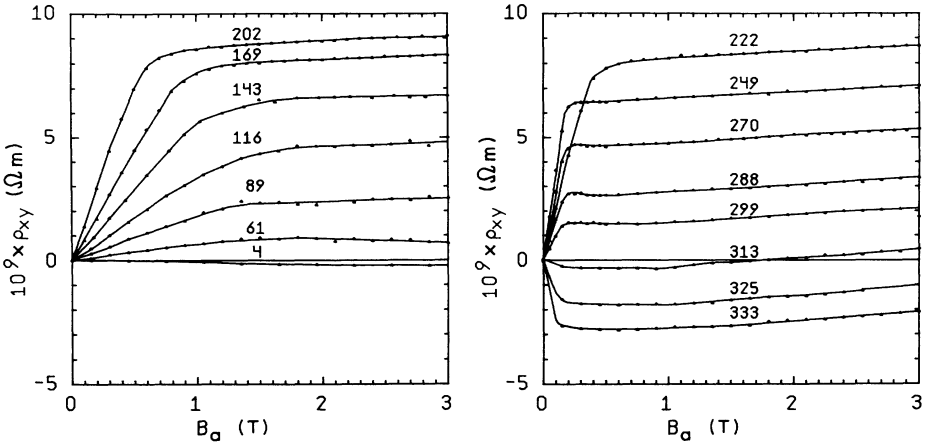

FIG. 8. Hall resistivity ρ_{xy} of a single crystal of Mn_2Sb at various temperatures.

III. ELECTRONIC STRUCTURE

A. Preliminaries

Ab initio spin-polarized band-structure calculations were performed using the self-consistent augmented-spherical-wave (ASW) method of Williams, Kübler, and Gelatt.[30] The local-density approximation was used as given by von Barth and Hedin.[31] Scalar relativistic effects were used as described by Methfessel and Kübler.[32] The spin-orbit coupling was not included in the calculations. For Mn $3d$ electrons, the spin-orbit interaction is small. For Sb $5p$ electrons, the spin-orbit interaction is large. However, the influence of spin-orbit interactions on the band structure is not expected to be large (expect perhaps at a few high-symmetry points in the Brillouin zone) because of quenching of the orbital angular momentum and the large exchange splitting.[33]

B. Band structure of Mn_2Sb

The band structure of Mn_2Sb was calculated using the unit-cell parameters $a = 4.051$ Å and $c = 6.537$ Å given by Darnell *et al.*[10] for $T = 200$ K. The Brillouin zone of Mn_2Sb is shown in Fig. 11. For Wigner-Seitz radii, we chose the values 1.429 Å for the Mn(1) and Mn(2) atoms, and 1.772 Å for Sb. In order to avoid a large overlap of adjacent spheres, empty spheres with radius 1.120 Å were included at positions $(0,0,c/2)$ and $(\frac{1}{2},\frac{1}{2},c/2)$. The basis functions were $3d$, $4s$, and $4p$ orbitals for Mn and $5s$, $5p$, and $5d$ orbitals for Sb. The $4f$ orbitals were included for Mn and Sb in the internal summation of the three center contributions to the matrix elements, which can be regarded as treating these as a perturbation.

The band structure of ferrimagnetic Mn_2Sb is shown in Fig. 12 for spin-up and spin-down electrons. The electronic structure is quite complex but clearly shows that Mn_2Sb is metallic and magnetic. The total density of states (DOS) and the contribution of the constituent atoms to the DOS are given in Fig. 13.

The feature at about 10 eV below the Fermi energy is due to a band consisting almost entirely of Sb $5s$ states. The Sb $5p$ band is very broad (it extends from -6 to $+6$ eV) and hybridizes strongly with Mn $3d$ states. The peak between -6 and -5 eV consists of Sb $5p$ states strongly mixed with Mn $4s$ states.

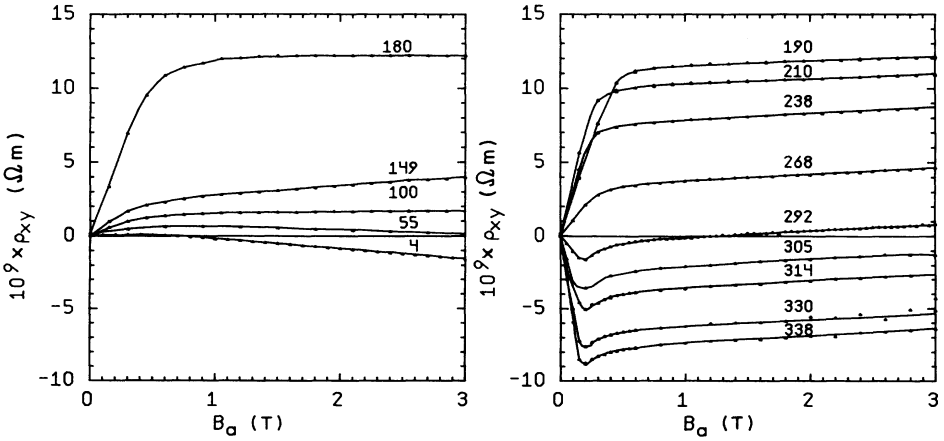

FIG. 9. Hall resistivity ρ_{xy} of a single crystal of $Mn_{1.96}Cr_{0.04}Sb$ at various temperatures.

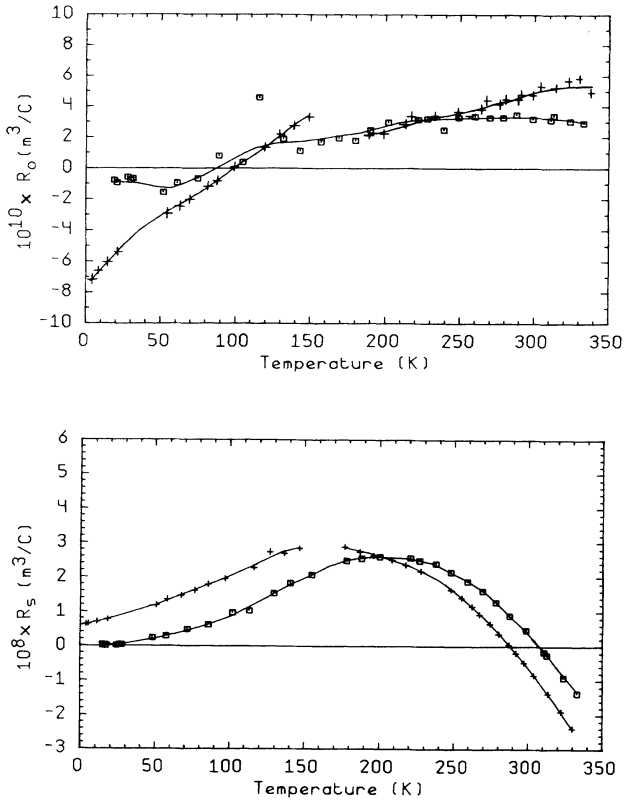

FIG. 10. Normal and anomalous Hall coefficients R_0 and R_s for single crystals of Mn_2Sb (open circles) and $Mn_{1.96}Cr_{0.04}Sb$ (solid circles) as a function of temperature.

The Mn $3d$ bands are very different for the two spin directions, and the calculations clearly show the ferrimagnetic character of Mn_2Sb, with antiparallel magnetic moments on Mn(1) and Mn(2) atoms (Fig. 13). By comparing the partial DOS for spin-up and spin-down $3d$ electrons, we deduce values for the intra-atomic exchange splitting ΔE_x of approximately 2.3 eV for Mn(1) and 3.6 eV for Mn(2). The numbers of spin-up and spin-down $3d$ electrons on Mn(1) are 1.70 and 4.01, respectively, leading to a magnetic moment of the $3d$ electrons of $\mu_d = -2.31\mu_B$. There is also a small magnetic moment of $-0.02\mu_B$ for the $4s$ and $-0.02\mu_B$ for the $4p$ electrons, so that the total moment on Mn(1) is $-2.35\mu_B$. The electronic configuration of Mn(1) is $3d^{5.71}4s^{0.51}4p^{0.65}$, the net charge (in the Wigner-Seitz sphere) is $+0.09$.

For Mn(2) atoms there are 4.47 and 0.89 spin-up and

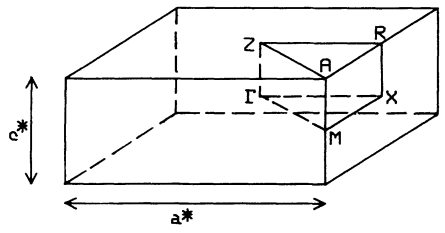

FIG. 11. The first Brillouin zone of Mn_2Sb showing the points of high symmetry.

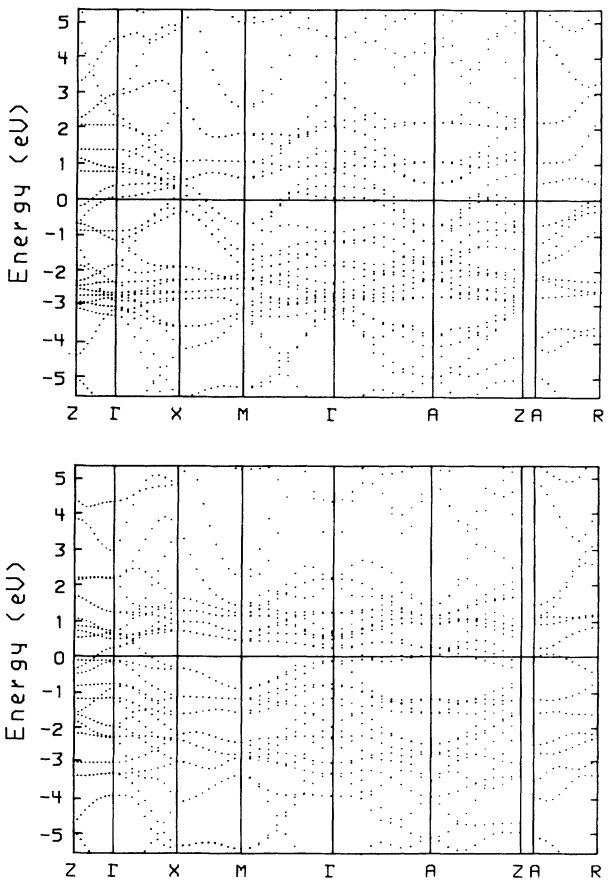

FIG. 12. Band structure of ferrimagnetic Mn_2Sb for spin-up electrons (upper part) and spin-down electrons (lower part).

spin-down electrons, respectively, leading to a magnetic moment of the $3d$ electrons of $\mu_d = +3.58\mu_B$. The $4s$ and $4p$ electrons on Mn(2) give moments of $+0.07\mu_B$ and $+0.05\mu_B$, respectively, so that the total magnetic moment on Mn(2) is $+3.71\mu_B$. The electronic configuration of Mn(2) is $3d^{5.36}4s^{0.40}4p^{0.48}$, the net charge (in the

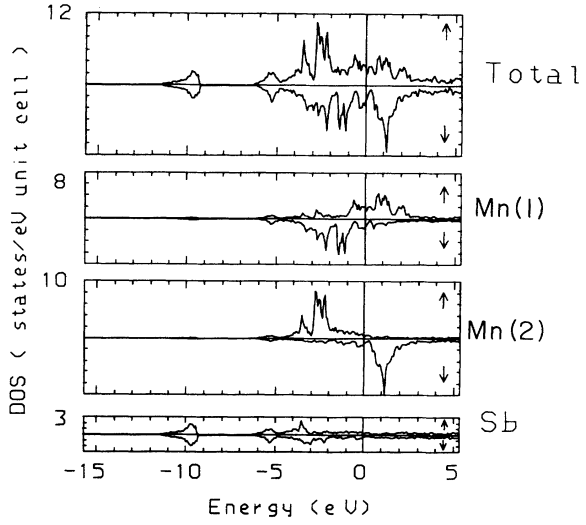

FIG. 13. DOS of ferrimagnetic Mn_2Sb and the partial DOS of the constituent atoms.

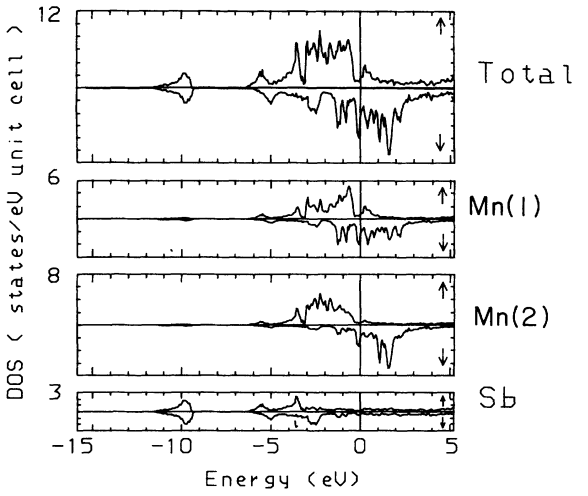

FIG. 14. DOS of ferromagnetic Mn_2Sb and the partial DOS of the constituent atoms.

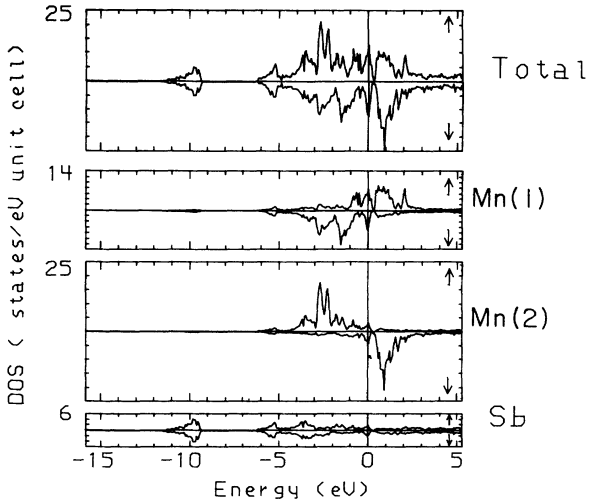

FIG. 15. DOS of antiferromagnetic Mn_2Sb and the partial DOS of the constituent atoms (for the double unit cell).

Wigner-Seitz Sphere) is +0.67. We remark that the value of the net charge depends strongly on the value of the Wigner-Seitz radius chosen, which is rather arbitrary. However, the calculated values indicate a more positive charge on Mn(2) atoms.

The calculated values of the $3d$ magnetic moments of $-2.31\mu_B$ on Mn(1) and $+3.58\mu_B$ on Mn(2) should be compared with the values $-2.1\mu_B$ and $+3.9\mu_B$,[3] or $-1.77\mu_B$ and $+3.55\mu_B$ (Ref. 4) for Mn(1) and Mn(2), respectively, obtained from neutron diffraction.

The magnetic moment on Sb is $+0.04\mu_B$. The calculated value of the total magnetic moment is $1.4\mu_B$ per formula unit Mn_2Sb, in reasonable agreement with the observed value of $1.8\mu_B$.[1,2]

We also calculated the band structure for a ferromagnetic spin alignment of Mn_2Sb. This calculation was started with a parallel alignment of the magnetic moments on Mn(1) and Mn(2), and was found to converge indeed to a (meta)stable ferromagnetic state. The fact that the calculations for both the ferrimagnetic (FI) and the ferromagnetic (F) states converge is an indication that the two magnetic structures are separated by an appreciable energy barrier. Finally, we calculated the band structure of an antiferromagnetic (AF) structure of Mn_2Sb, in which there is an antiparallel ordering of the moments on adjacent triple layers Mn(2)-Mn(1)-Mn(2) (see Fig. 1). This calculation also converged readily. The resulting DOS and partial DOS of the F and AF states of Mn_2Sb are represented in Figs. 14 and 15. In the AF structure the unit cell contains two triple layers A and B with antiparallel magnetic moments. For symmetry reasons the DOS for spin-up electrons in A is equal to the DOS for spin-down electrons in B. In Fig. 15 we represent as DOS the sum of the DOS of spin-up electrons on A and spin-down electrons on B. Characteristic values for the electronic configuration of the Mn(1) and Mn(2) atoms are given in Table I.

By comparing these band structures (Figs. 13–15), we notice significant differences in hybridization in the F, FI, and AF states, which are important for explaining the interatomic exchange interactions. For example, in the FI structure there is a peak at −3.5 eV with hybridization of Sb $5p$ and Mn(2) $3d$ states. The Mn(1) $3d$ electrons are not involved in this peak because they have the

TABLE I. Number of Mn $3d$ electrons n_d, magnetic moment on Mn μ_d, exchange splitting ΔE_x, and the ratio $I=\Delta E_x/\mu$ for Mn in intermetallic compounds.

		n_d	μ_d/μ_B	ΔE_x (eV)	$I=\Delta E_x/\mu$	Ref.
Mn_2Sb (FI)	Mn(1)	5.71	2.31	2.30	1.00	
	Mn(2)	5.36	3.58	3.60	1.00	
Mn_2Sb (F)	Mn(1)	5.74	2.04	2.00	0.98	
	Mn(2)	5.42	3.46	3.30	0.96	
Mn_2Sb (AF)	Mn(1)	5.72	2.28	2.10	0.92	
	Mn(2)	5.37	3.51	3.40	0.97	
MnSb (F)	Mn	5.50	3.24	3.50	1.08	34
MnSb (AF)	Mn	5.49	3.16	3.00	0.95	34

opposite spin direction. However, the situation is different for the F structure; now the magnetic moments of Mn(1) and Mn(2) 3*d* electrons are parallel, and we see indeed that in the −3.5-eV peak for the F structure both Sb 5*p*, Mn(1) 3*d*, and Mn(2) 3*d* orbitals participate.

Generally the DOS curves and hybridizations are very similar for the AF and FI structures, and differ from the F structure. A different feature in the band structure of the AF state is a sharp peak in the DOS at the Fermi energy (Fig. 15) due to a band with very little dispersion.

The ferrimagnetic to antiferromagnetic phase transition in $Mn_{2-x}Cr_xSb$ is accompanied by a change of the lattice parameters, and the phase transition occurs at the same critical value of the *c* axis $c_0=6.53$ Å for all chromium concentrations. In order to find out whether a small change of the lattice parameters leads to a significant change of the band structure, we also carried out a band-structure calculation of Mn_2Sb for the parameters $a=4.082$ Å, $c=6.513$ Å (these values are typical for antiferromagnetic $Mn_{1.9}Cr_{0.1}Sb$). However, we found that the differences with the band structure of Mn_2Sb for $a=4.08$ Å, $c=6.56$ Å are quite small (differences in n_d and μ_d values smaller than 0.05).

C. Magnetic interactions in Mn_2Sb

In Table I we compare data for intermetallic compounds containing Mn and Sb. We find that the number of Mn 3*d* electrons is nearly the same for all compounds but that the magnetic moments of the Mn atoms vary strongly. We observe that there is a simple relation between the exchange splitting ΔE_x and the magnetic moment μ_d of the *d* electrons on Mn; in fact, the ratio $I=\Delta E_x/\mu_d$ is nearly the same for all compounds, and does not depend on the type of magnetic order in MnSb and Mn_2Sb.

The intra-atomic exchange interaction between Mn 3*d* electrons can be expressed in terms of the average interaction between parallel spins $J=\frac{1}{14}(F^{(2)}+F^{(4)})$ ($F^{(2)}$ and $F^{(4)}$ are Slater parameters). With the values $F^{(2)}=8.72$ eV and $F^{(4)}=5.20$ eV,[35] one obtains $J=0.99$ eV. The semiempirical relation $J=0.59+0.075(Z-21)$ (Ref. 36) gives for Mn ($Z=25$) a value $J=0.89$ eV. If intra-atomic exchange interactions are the origin of the exchange splitting between spin-up and spin-down bands, one expects $I=\Delta E_x/\mu_d$ to be equal to *J*. The fact that the values of *I* obtained from band-structure calculations are very close to the atomic parameter *J* proves that the exchange splitting between Mn 3*d* bands is mainly an intra-atomic effect.

A comparison of the DOS of FI and F Mn_2Sb gives information about the inter-atomic exchange interactions between the Mn atoms. Hybridization between orbitals of different atoms leads to a direct exchange interaction. Generally hybridization also leads to a broadening of the energy bands. In FI Mn_2Sb the moments on Mn(1) and Mn(2) are antiparallel. A consequence is that hybridization between Mn(1) and Mn(2) 3*d* electrons in FI Mn_2Sb (and also in AF Mn_2Sb) is not as strong as in F Mn_2Sb. The reason is that there are not many states of the same spin direction and at the same energy of the neighboring atom to hybridize with in the FI and AF cases as there are for the F structure. We find, indeed, in the DOS of F Mn_2Sb that the occupied Mn(2) 3*d* states form a broader band than in the FI state, as a result of strong hybridization between Mn(2) $d^{\uparrow}$ and Mn(1) $d^{\uparrow}$ states. A hybridization of this type is not possible in F Mn_2Sb. The unoccupied Mn(2) $d^{\downarrow}$ states for F are broader than for FI because of hybridization of Mn(2) $d^{\downarrow}$ with Mn(1) $d^{\downarrow}$. The same trends are seen when comparing F and AF. These considerations show that Mn(1) and Mn(2) *d* states hybridize mainly within one triple layer Mn(2)-Mn(1)-Mn(2). The hybridization is hardly influenced by the relative orientation of the magnetic moments of adjacent triple layers (i.e., the change from FI to AF Mn_2Sb).

In Mn_2Sb the Mn 3*d* states are close to being half-filled. For a half-filled *d* band the tendency for magnetic moment formation is a maximum because the gain of intra-atomic exchange energy is a maximum for this case. Hybridization of half-filled bands favors antiparallel moment alignment,[37–39] as illustrated in Fig. 16. Hybridization of two half-filled *d* bands leads to lower energy in the AF case but not in the F case.

From the similarity of the DOS of Mn(2) in the FI and AF states, it is concluded that the direct Mn(2)-Mn(2) exchange between adjacent triple layers is weak. However, we expect also an indirect exchange coupling via the partly filled Sb 5*p* states between adjacent triple layers.

D. Interpretation of transport properties in terms of the band structure

In this section we try to understand the change of the transport properties at the phase transition in $Mn_{2-x}Cr_xSb$ by comparing the Fermi surfaces of the ferrimagnetic and antiferromagnetic states of Mn_2Sb. The

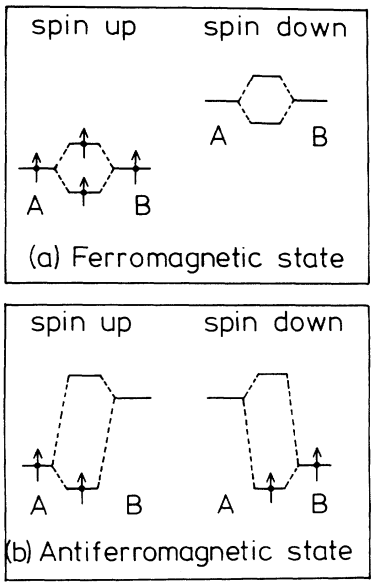

FIG. 16. Covalent inter-atomic interactions between two atoms *A* and *B* for the (a) ferromagnetic and (b) the antiferromagnetic state.

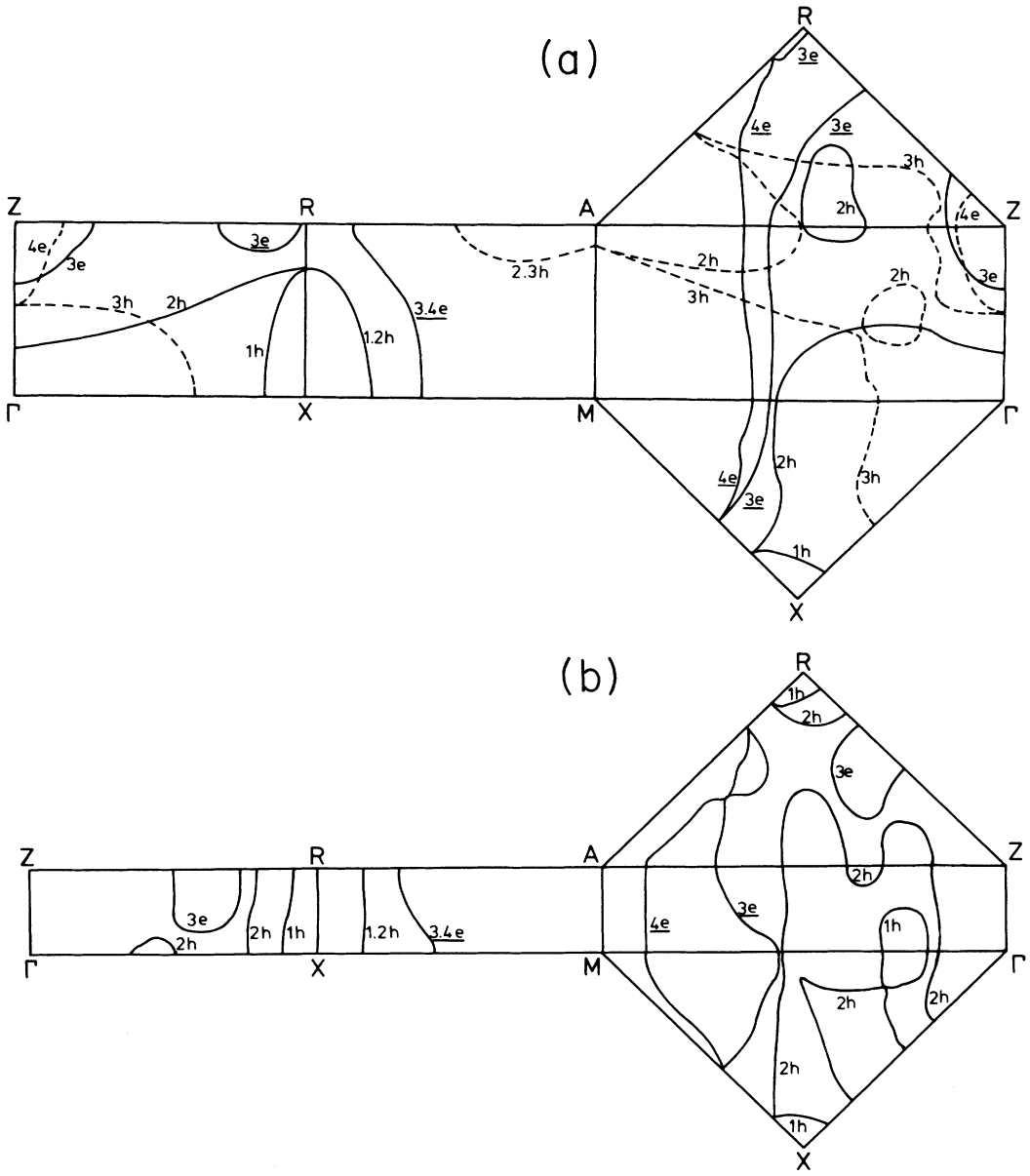

FIG. 17. Intersections of the Fermi surface with the boundary planes of an irreducible part of the Brillouin zone. The numbers of the orbits correspond to the energy order of the bands; electron and hole orbits are indicated by *e* and *h*, respectively. (a) Ferrimagnetic Mn_2Sb; solid lines for spin-up and dotted lines for spin-down electrons (upper part). (b) Antiferromagnetic Mn_2Sb (lower part).

TABLE II. Number of *d* electrons n_d and magnetic moment μ_d on sites 1 and 2, and the total moment μ_d (total), for a virtual crystal $Mn_{1.9}Cr_{0.1}Sb$, in which Cr is substituted on site 1 or 2. The data are compared with values for FI Mn_2Sb.

		$Mn_{1.9}Cr_{0.1}Sb$	
	Mn_2Sb	Cr on site 1	Cr on site 2
site 1 n_d	5.71	5.63	5.72
μ_d	2.31	2.23	2.38
site 2 n_d	5.36	5.36	5.26
μ_d	3.58	3.62	3.64
μ_d (tot)	1.27	1.39	1.26

intersections of the Fermi surface with the boundary planes of an irreducible part of the Brillouin zone are shown in Fig. 17. A given band can intersect the Fermi level at different places in the Brillouin zone leading to several orbits (open or closed) for the same band index n. Most of the orbits are hole type. However, there are two large electron orbits ($3e$ and $4e$) around the line AM in the FI and AF phases. In FI Mn_2Sb these electron orbits are present only for spin-up electrons. In AF Mn_2Sb the ($3e$,$4e$) orbits are present for the two spin directions. The Hall effect and the Seebeck effect of FI Mn_2Sb have a different sign, which indicates the contribution of electrons and holes to the transport properties. This is consistent with the calculated band structure which shows indeed electron and hole sheets at the Fermi level.

The electrons in orbitals ($3e$,$4e$) in AF Mn_2Sb have a large effective mass (they correspond to the narrow band with little dispersion at the Fermi level, mentioned already in Sec. III B) and will give a large negative contribution to the Seebeck effect. Assuming that the electronic structure of $Mn_{2-x}Cr_xSb$ is nearly the same as that of Mn_2Sb, this explains the large negative Seebeck effect of AF $Mn_{2-x}Cr_xSb$ (Fig. 7). The dispersion of the energy bands at the Fermi energy is generally larger for the FI than for the AF phase. Thus, the effective mass of the charge carriers will be larger in the AF phase, and this explains the smaller electrical conductivity in the AF phase (Fig. 5).

E. Virtual crystal band-structure calculations of $Mn_{1.9}Cr_{0.1}Sb$

In order to investigate the influence on the band structure of the reduced electron concentration in $Mn_{2-x}Cr_xSb$ due to the Cr substitution, we performed so-called virtual crystal calculations, in which a virtual atom with atomic number 25-x is placed on site Mn(1) or Mn(2). The results of the calculations are given in Table II.

Magnetic measurements indicate that the magnetization of $Mn_{2-x}Cr_xSb$ is (slightly) smaller than that of Mn_2Sb.[10] This could be the result of an increased moment on site 1 or a decreased moment on site 2, as compared with Mn_2Sb. The calculated magnetic moments show that only a substitution of Cr on site 2 is consistent with the experimental data. Neutron-diffraction data[3] appear to indicate that Cr occupies type-1 sites. However, more accurate data are needed to obtain conclusive evidence.

IV. CONCLUDING REMARKS

It has been possible to carry out band-structure calculations for different ordered magnetic structures (FI, F, and AF) of Mn_2Sb. The lowest total energy was obtained for FI Mn_2Sb in agreement with experimental observation. The energy differences between the magnetic structures are not sufficiently reliable for calculations of the strength of magnetic exchange interactions. It was found that the local charge on the atoms is hardly influenced by the magnetic order: the number n_d of $3d$ electrons on the Mn atoms is nearly the same for the FI, F, and AF structures. However, the type of magnetic order leads to appreciable variations, of the order of $(0.1-0.3)\mu_B$, of the local magnetic moments on Mn.

The band structures of the FI, AF, and F states of Mn_2Sb show characteristic differences in bandwidth and hybridization, in particular for the $3d$ bands of Mn(1) and Mn(2) atoms. The hybridization (covalent mixing) between $3d$ orbitals of Mn(1) and Mn(2) atoms is responsible for the strong, direct antiferromagnetic exchange within the Mn(2)-Mn(1)-Mn(2) triple layers. The orientation of the magnetic moments of two adjacent triple layers (AF or FI structures) is determined by a small direct exchange and an indirect exchange via Sb $5p$ states. These exchange contributions are fairly weak, and the phase transition AF→FI in chromium-doped crystals shows that the strength of this exchange depends strongly on the lattice constant, and changes sign at a critical value c_0. The indirect exchange will have a ferromagnetic contribution involving the partly occupied Sb $5p$ band. An interaction of this type is responsible for the strong ferromagnetism in the Heusler alloys NiMnSb, PtMnSb,[40–42] and in MnSb.[34]

In addition to the ferromagnetic contribution which is present only for a partly occupied Sb $5p$ band, there will also be an antiferromagnetic superexchange-type interaction between two Mn(2) atoms via Sb $5p$. Strictly speaking, the ferromagnetic and antiferromagnetic contributions cannot be separated theoretically.

The phase transition AF→FI in $Mn_{2-x}Cr_xSb$ strongly influences the transport properties: the resistivity decreases, the Seebeck effect changes from negative to positive values. These observations are explained by the calculated band structure of the FI and AF structures; they are a consequence of a narrow electronlike band at the Fermi energy in the AF state.

Finally, we mention a complication due to deviations from the stoichiometric composition of Mn_2Sb. It is found that samples of Mn_2Sb, grown from stoichiometric amounts of the elements, contain some MnSb as a second phase. This is due to the fact that stoichiometric Mn_2Sb is stable only at high temperatures (900 K).[43,44] Cooling to lower temperatures leads to precipitation of some MnSb, and a remaining Mn_2Sb phase which contains some excess Mn, probably present at the interstitial sites between triple layers [positions $(0,0,\frac{1}{2})$ and $(\frac{1}{2},\frac{1}{2},\frac{1}{2})$]. The nonstoichiometry of the Mn_2Sb phase can be influenced by annealing and quenching procedures. The presence of a small amount of interstitial Mn(i) will contribute to a parallel alignment of the magnetic moments of adjacent triple layers [the Mn(i)-Mn(2) interaction is presumably antiferromagnetic, like the interaction Mn(1)-Mn(2); the Mn(i)-Mn(2) leads to an effective ferromagnetic coupling between magnetic moments of Mn(2) of adjacent triple layers]. The presence of interstitial Mn(i) will also influence the transport properties. Further experimental work is necessary to determine the occupancy of interstitial sites by Mn or Cr, as a result of

nonstoichiometry, native atomic disorder, and Cr substitution.

ACKNOWLEDGMENTS

The authors gratefully acknowledge financial support for this investigation from Philips Research Laboratories, Eindhoven. This investigation was supported by the Stichting voor Fundamental Onderzoek der Materie (FOM) with financial aid from the Netherlands Organization for the Advancement of Research (NWO).

*Present address: Lab. für Festkörperphysik, ETH Hönggerberg, 8093 Zürich, Switzerland.

[1]Leroy Heaton and N. S. Gingrich, Acta Crystallogr. **8**, 207 (1955).

[2]M. K. Wilkinson, N. S. Gingrich, and C. G. Shull, J. Phys. Chem. Solids **2**, 289 (1957).

[3]A. E. Austin, E. Adelson, and W. H. Cloud, Phys. Rev. **131**, 1511 (1963).

[4]H. A. Alperin, P. J. Brown, and R. Nathan, J. Appl. Phys. **34**, 1201 (1963).

[5]T. J. Swodoba, W. H. Cloud, T. A. Bither, M. S. Stadler, and H. S. Jarrett, Phys. Rev. Lett. **4**, 509 (1960).

[6]T. Kanomata and H. Ido, J. Appl. Phys. **55**, 2039 (1984).

[7]W. H. Cloud, H. S. Jarrett, A. E. Austin, and E. Adelson, Phys. Rev. **120**, 1969 (1960).

[8]P. E. Biersted, F. J. Darnell, W. H. Cloud, R. B. Flippen, and H. S. Jarrett, Phys. Rev. Lett. **8**, 15 (1962).

[9]P. Bierstedt, Phys. Rev. **132**, 669 (1963).

[10]F. J. Darnell, W. H. Cloud, and H. S. Jarrett, Phys. Rev. **130**, 647 (1963).

[11]S. Ooshima, T. Wakiyama, and T. Anayama, Jpn. J. Appl. Phys. **17**, 659 (1978).

[12]S. Ooshima, K. Fudamich, T. Wakiyama, and T. Anayama, Jpn. J. Appl. Phys. **18**, 707 (1979).

[13]R. W. Houghton and W. Weyhmann, Phys. Rev. Lett. **20**, 842 (1968).

[14]C. Blaauw, G. R. Mackay, and W. Leiper, Phys. Lett. **62A**, 129 (1977).

[15]C. Blaauw, G. R. Mackay, and W. Leiper, J. Magn. Magn. Mater. **7**, 234 (1978).

[16]C. Blaauw, G. R. Mackay, and W. Leiper, J. Magn. Magn. Mater. **8**, 240 (1978).

[17]K. V. S. Rama Rao, S. L. Pinjare, T. Rajasekharan, and C. Ramasastry, J. Phys. Chem. Solids **41**, 7 (1980).

[18]S. L. Pinjare and K. V. S. Rama Rao, J. Phys. F **14**, 2185 (1984).

[19]N. N. Delyagin, V. I. Nesterov, and A. K. Churakov, Zh. Eksp. Teor. Fiz. **93**, 1480 (1987) [Sov. Phys. JETP **66**, 844 (1987)].

[20]S. Funahashi and N. Kazama, J. Phys. Soc. Jpn. **41**, 811 (1976).

[21]S. Funahashi and Y. Hamaguchi, J. Magn. Magn. Mater. **15-18**, 353 (1980).

[22]K. Sato, M. Nakazima, T. Miyazaki, Y. Isikawa, and K. Mori, J. Appl. Phys. **55**, 2036 (1984).

[23]C. Kittel, Phys. Rev. **120**, 335 (1960).

[24]H. S. Jarrett, Phys. Rev. **134**, A952 (1964).

[25]J. D. Wolf and J. E. Hanton, J. Appl. Phys. **32**, 2584 (1961).

[26]L. Berger and G. Bergmann, in *The Hall Effect and its Applications,* edited by C. L. Chien and C. R. Westgate (Plenum, New York, 1980).

[27]M. J. Otto, Ph.D. thesis, University of Groningen, 1987.

[28]M. J. Otto, R. A. M. van Woerden, P. J. van der Valk, J. Wijngaard, C. F. van Bruggen, and C. Haas, J. Phys.: Condens. Matter **1**, 2351 (1989).

[29]J. H. Wijngaard, Ph.D. thesis, University of Groningen, 1991.

[30]A. R. Williams, J. Kübler, and C. D. Gelatt, Jr., Phys. Rev. B **19**, 6094 (1979).

[31]U. von Barth and L. Hedin, J. Phys. C **5**, 1629 (1972).

[32]M. Methfessel and J. Kübler, J. Phys. F **12**, 141 (1982).

[33]R. Coehoorn and R. A. de Groot, J. Phys. F **15**, 2135 (1985).

[34]R. Coehoorn, C. Haas, and R. A. de Groot, Phys. Rev. B **31**, 1980 (1985).

[35]J. S. Griffith, *The Theory of Transition Metal Ions* (Cambridge University Press, Cambridge, 1961).

[36]D. van der Marel and G. A. Sawatzky, Phys. Rev. B **37**, 10 674 (1988).

[37]J. Kübler, A. R. Williams, and C. B. Sommers, Phys. Rev. B **28**, 1745 (1983).

[38]A. R. Williams, R. Zeller, V. I. Moruzzi, C. D. Gelatt, Jr., and J. Kübler, J. Appl. Phys. **52**, 2067 (1981).

[39]A. R. Williams, V. I. Moruzzi, C. D. Gelatt, Jr., J. Kübler, and K. Schwarz, J. Appl. Phys. **53**, 2019 (1982).

[40]R. A. de Groot, F. M. Mueller, P. G. van Engen, and K. H. J. Buschow, Phys. Rev. Lett. **50**, 2024 (1983).

[41]R. A. de Groot, F. M. Mueller, P. G. van Engen, and K. H. J. Buschow, J. Appl. Phys. **55**, 2151 (1984).

[42]M. J. Otto, R. A. M. van Woerden, P. J. van der Valk, J. H. Wijngaard, C. F. van Bruggen, C. Haas, and K. H. J. Buschow, J. Phys. Condens. Matter **1**, 2341 (1989).

[43]N. E. Askheim and F. Grönvold, J. Chem. Thermodyn. **1**, 153 (1969).

[44]V. M. Ryzhkovskii, N. D. Zhigadlo, and I. L. Pashkovskii, Cryst. Res. Technol. **25**, 165 (1990).